COBEM 2023 27TH INTERNATIONAL CONGRESS OF MECHANICAL ENGINEERING

ABCM Brazilian Society of Mechanical Sciences and Engineering
27th ABCM International Congress of Mechanical Engineering
December 04-08, 2023, Florianópolis-SC, Brazil

COB-2023-1077
NUMERICAL MODELLING OF A DIRECT REFRIGERANT TWO-PHASE COOLING SYSTEM FOR THE THERMAL MANAGEMENT OF ELECTRIC VEHICLE BATTERY

Ernane Silva
TEG Thermofluids Engineering Group, Universidade Federal de Santa Catarina, 89219600, Joinville, SC, Brazil
ernane.silva@teg.ufsc.br

Thiago Dutra
TEG Thermofluids Engineering Group, Universidade Federal de Santa Catarina, 88905120, Araranguá, SC, Brazil
thiago.dutra@teg.ufsc.br

Abstract. *The heating of battery cells represents one of the most challenging aspects for the development of electric vehicles, since higher temperatures reduce their life, performance and safety. Nowadays, lithium-ion batteries are seen as the most prominent energy storage devices for this application and generate heat due to different physical and chemical processes that occur during charge and discharge periods. In order to avoid the battery cells to overheat and to increase mileage of current electric vehicles, several thermal management systems have been developed, some of which are based on the vapor compression cycle. Among them, the direct refrigerant two-phase cooling is seen as a promising technology due to its superior cooling performance when compared to cabin air cooling systems and reduced complexity and weight when compared to secondary liquid loop cooling systems. It consists of extending the vehicle AC system by including an additional evaporator in the battery, usually named cooling plate, in parallel with the cabin evaporator. The adoption of numerical models for the design of these systems is of paramount importance, since plenty of configurations can be simulated without the expense of experimental tasks. This study presents a comprehensive simulation model for direct refrigerant two-phase cooling systems applied for the thermal management of lithium-ion batteries used in electric vehicles. The refrigeration system under analysis is composed of compressor, condenser, expansion device and two evaporators, one for cooling of the cabin air and the other for battery cooling, the latter being in direct contact with the battery cells. In the numerical model, the compressor is represented by means of volumetric and overall isentropic efficiencies, the expansion device is described by an orifice equation and the heat exchangers are simulated using multi-zone models. The results reveal how the system operational parameters change as a function of the variable cooling load.*

Keywords: *Electric vehicle, Battery thermal management, Air conditioning*

1. INTRODUCTION

The interest in electric vehicles has increased significantly, boosted mainly by more restrictive environmental regulations on greenhouse gas emissions. Rechargeable lithium-ion batteries are regarded as the most suitable energy storage devices for electric vehicles due to their higher energy density, higher specific power, lighter weight, lower self-discharge rates, higher recyclability and longer cycle life than other rechargeable batteries. However, the performance, life and safety of Li-ion batteries are very sensitive to temperature (Liu *et al.*, 2017). Pesaran (2002) and Pesaran *et al.* (2013) indicated that the operating temperature of these devices should be in the 15 – 35 °C range and that the maximum temperature difference between the battery modules should not exceed 5 °C in order to avoid adverse effects.

According to Thomas and Newman (2003), lithium-ion batteries generate heat by reversible entropy, resistive dissipation, relaxation of the concentration gradient of the cell, and chemical reaction. These processes occur during charge and discharge periods and increase the battery temperature if heat is not properly released. In order to avoid the battery cells to overheat and to increase mileage of current electric vehicles, several battery thermal management systems (BTMS) have been developed (Kim *et al.*, 2019), some of which are based on the vapor compression cycle (Figure 1). In the cabin air cooling system (Figure 1a), part of the cold air from the cabin is directed towards the battery. Although very simple, such system is limited by the low heat capacity of air, which means that large air flow rates would be required under intense heat generation. The adoption of secondary loop liquid cooling (Figure 1b) is an effective mean of dealing with such problem. However, the system complexity and weight increase considerably. An alternative to both system architectures is the direct refrigerant two-phase cooling (Figure 1c), in which an additional evaporator, usually named cooling plate, is included in the AC system in parallel to the cabin evaporator and in direct contact with the battery. This system takes advantage of the large latent heat of refrigerants to avoid large refrigerant flow rates. Besides, few additional components are required in the system, which include the cooling plate, another expansion device, and tubes.

This study aims to develop and validate a comprehensive simulation model for direct refrigerant two-phase cooling systems applied for the thermal management of lithium-ion batteries used in electric vehicles. A sensitivity analysis is also conducted to verify how performance parameters change with the compressor speed and the heat generated in the battery.

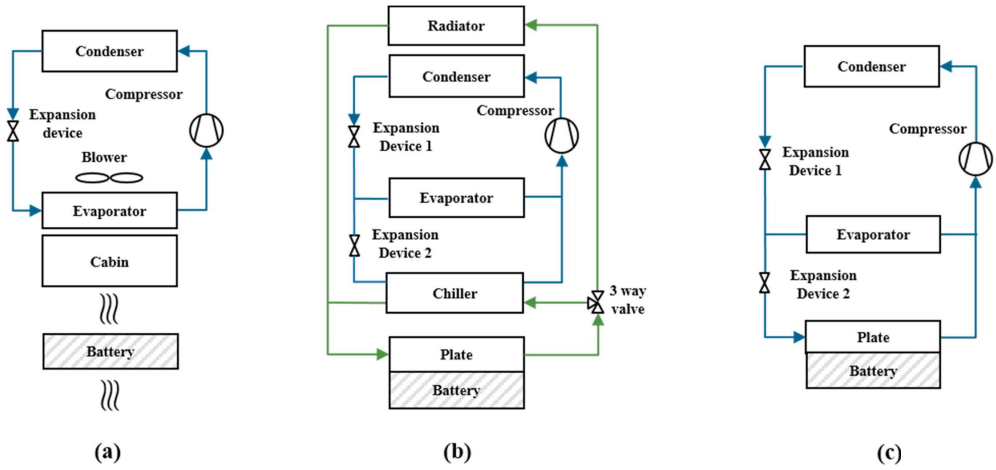

Figure 1. Battery thermal management systems based on the vapor compression cycle: a) cabin air cooling, b) secondary loop liquid cooling, and c) direct refrigerant two-phase cooling. Adapted from Kim *et al.* (2019).

2. MATHEMATICAL MODEL OF THE BTMS

The BTMS under analysis is composed of compressor, condenser, two electronic expansion valves and two evaporators, one for cooling of the cabin air and the other one for battery cooling, the latter being in direct contact with the battery cells (Figure 1c). In the numerical model, the compressor is represented by means of volumetric and overall isentropic efficiencies, the expansion device is described by a single-phase orifice equation and the heat exchangers are simulated using multi-zone models. These components are integrated by means of the generic simulation model proposed by Zhu *et al.* (2013) for performance and control analysis of variable refrigerant flow (VRF) systems. The subcooling degree at the condenser outlet is an input parameter of the model and the evaporating pressure, condensing pressure, and the superheating degree at the evaporator outlet remain as the only unknowns once the operating conditions (mass flow rates of air in the condenser and cabin evaporator, thermodynamic states of air at the inlet of the condenser and cabin evaporator, and the battery temperature) are defined. This method respects the mass and energy conservation as well as the pressure continuity in each point of the refrigerant circuit while avoiding extensive numerical iterations associated with the determination of the refrigerant distribution in the system.

2.1 Compressor

The compressor sub-model provides the refrigerant mass flow rate, power consumption and refrigerant enthalpy at the discharge line. The mass flow rate is calculated as

$$\dot{m} = \eta_v \rho_1 V_{sw} f, \tag{1}$$

where ρ_1 stands for the refrigerant density at the compressor suction line, V_{sw} is the compressor displacement, f is the compressor speed and η_v is the volumetric efficiency, which can be obtained from performance data provided by the compressor manufacturer.

The compressor power consumption can be determined in a similar fashion by means of the compressor overall isentropic efficiency, η_s, as

$$\dot{W} = \frac{\dot{m}\,(h_{2,s} - h_1)}{\eta_s}, \tag{2}$$

where h_1 is the refrigerant enthalpy at the compressor suction line and $h_{2,s}$ is the refrigerant enthalpy at the compressor discharge line after an isentropic compression process. Values of η_s can also be obtained from performance data provided by the compressor manufacturer. The refrigerant enthalpy at the compressor discharge line, h_2, is calculated from an energy balance at the compressor shell assuming that the heat released to the environment is negligible, that is,

$$h_2 = h_1 + \frac{\dot{W}}{\dot{m}}. \tag{3}$$

The refrigerant enthalpy at the compressor suction line, h_1, is an input parameter for the compressor sub-model together with the evaporating and condensing pressures, p_e and p_c, respectively.

In the present study an electrical compressor with 33 cc of displacement was considered. The correlations provided in Eqs. (4) and (5) were fitted to experimental data provided by the manufacturer for 27 operating conditions with 1000 rpm $\leq f \leq$ 8500 rpm, 1.5 bar $\leq p_e \leq$ 8 bar, and 10 bar $\leq p_c \leq$ 25 bar. Maximum deviations of 1.9% and 3.4% in respect to experimental data were observed when such expressions are used to calculate mass flow rate and power consumption, respectively.

$$\eta_v = 1 + \left(\frac{282}{f^2 - 296f}\right)\left(\frac{p_c}{p_e}\right) \tag{4}$$

$$\eta_s = 0.505 + (0.0605 - 0.000291f)\left(\frac{p_c}{p_e}\right) - \left(\frac{0.234}{f}\right)\left(\frac{p_c}{p_e}\right)^2 \tag{5}$$

2.2 Electronic expansion valves

The refrigerant flow through the electronic expansion valve is described as an isenthalpic throttling process in which the refrigerant is expanded from condensing to evaporating pressure, with the mass flow rate calculated by means of the single-phase orifice equation (Nilpueng and Wongwises, 2012), that is,

$$\dot{m} = \phi C_v A_o \sqrt{2\rho_3 \Delta p}. \tag{6}$$

In Eq. (6) ϕ is the opening ratio of the valve, C_v is the flow coefficient, A_o is the orifice area, ρ_3 is the refrigerant density at the condenser outlet, and Δp is the pressure difference across the valve. In the present study valves with orifice diameter of 1.4 mm were considered. Predictions of mass flow rate using Eq. (6) and $C_v = 0.5253$ deviated less than 0.3% from the manufacturer data.

2.3 Heat exchangers

2.3.1 Condenser and cabin evaporator

In the present study, louvered fin-flat tube microchannel heat exchangers were adopted for both the condenser and cabin evaporator. The condenser is made of horizontal tubes with seven microchannels each and arranged in a single row with four passes, containing 14, 7, 6 and 4 tubes from inlet to outlet. The height and width of the condenser are 325 mm and 500 mm, respectively. The evaporator is made of two parallel sets of 24 vertical tubes with eleven microchannels each disposed in a counter flow arrangement. The height and width of the cabin evaporator are 220.7 mm and 233.6 mm, respectively. The complete geometrical description of the condenser and cabin evaporator are given in Datta *et al.* (2016) and Shi *et al.* (2011), respectively.

Zone models (Jabardo *et al.*, 2002; Ding, 2007; Cuevas *et al.*, 2009) were adopted for the condenser and cabin evaporator. In this sense, they were divided into zones associated with the phase of the refrigerant and each zone was treated as a separate heat exchanger. The condenser was divided into superheated, two-phase, and subcooled zones, while the cabin evaporator was divided into two-phase and superheated zones. Pressure losses and fluid maldistributions were neglected both in the refrigerant-side and air-side. The overall thermal conductance between air and refrigerant for each zone, UA, is defined as

$$\frac{1}{UA} = \frac{1}{\eta_a A_a h_a} + \frac{1}{\eta_r A_r h_r}, \tag{7}$$

where η, A, and h stand for the surface fin efficiency, the surface area, and the convective heat transfer coefficient, whereas the subscripts a and r indicate air-side and refrigerant-side, respectively. The thermal resistances due to tube-fin contact, wall conduction, and two-phase convection were assumed negligibly small. Therefore, the second term on the right hand side of Eq. (7) vanishes in the two-phase zone. The air-side heat transfer coefficient was determined from the generalized correlation for louver fin geometry proposed by Chang and Wang (1997), whereas the single-phase refrigerant-side heat transfer coefficient was calculated according to the constant heat flux condition for laminar flow and Gnielinski's correlation (Gnielinski, 1976) for turbulent flow.

The heat transfer rate for each zone was determined according to the ϵ-NTU method, by means of which it can be written as

$$Q = A\epsilon C_{min}\left(T_{h_i} - T_{c,i}\right), \tag{8}$$

where C_{min} is the smallest among the refrigerant and air-side thermal capacities, T_{h_i} is the inlet temperature of the hot fluid, and T_{c_i} is the inlet temperature of the cold fluid. The heat exchanger effectiveness is calculated according to

$$\epsilon = 1 - \exp\left\{\left(\frac{1}{C_r}\right) NTU^{0.22}\left[\exp(-C_r NTU^{0.78}) - 1\right]\right\}, \tag{9}$$

for single-phase zones and

$$\epsilon = 1 - \exp\left(-NTU\right), \tag{10}$$

for two-phase zones. The assumption of cross flow condition with both fluids not mixed, which has been widely adopted for the modeling of automotive heat exchangers (Jabardo *et al.*, 2002; Zhao *et al.*, 2012; Shojaeefard *et al.*, 2017), leads to the latter expressions for ϵ. In these equations, $NTU = UA/C_{min}$ is the number of transfer units and $C_r = C_{min}/C_{max}$ is the ratio between the refrigerant and air-side thermal capacities, where C_{max} is the largest among the refrigerant and air-side thermal capacities. In the evaporator, the dehumidification in the air side is considered assuming the straight-line law, that is, the thermodynamic state of air at the evaporator outlet must lie on the line joining its thermodynamic state at the inlet with the saturated state at the dew-point temperature.

The condenser and evaporator sub-models were validated against experimental data of heat transfer rate from Datta *et al.* (2016) and Shi *et al.* (2011), respectively. The numerical results for the condenser overestimate the experimental measurements by less than 2% for all conditions the condenser is not blocked in the experimental campaign. On the other hand, the numerical results generally underestimate the heat transfer rate in the evaporator, with an average deviation of 6.5% if the experiments with asymmetric deflector at the inlet manifold are not considered. These larger deviations can be attributed mainly to two aspects: (i) neglect of pressure loss and (ii) refrigerant maldistribution. Generally, pressure losses are more important for evaporator modeling because the pressure levels at the evaporator are lower than at the condenser. Refrigerant maldistribution is also a serious problem for the evaporator design since the refrigerant two-phase state at the evaporator inlet favors the non-homogenous heat transfer. Nevertheless, the results indicate a good accuracy at a very low computational cost for the prediction of the heat transfer rate in the heat exchangers.

2.3.2 Battery evaporator

The battery evaporator is a flat tube microchannel heat exchanger with eight parallel horizontal tubes positioned at the bottom of the battery, which is made of an arrangement of 4 x 24 Samsung SDI 94Ah cells with dimensions 173 mm x 125 mm x 45 mm. In the absence of information from the manufacturer, the thermal conductivity of the battery cell is assumed 25 W/(mK) (Javani *et al.*, 2014). The flat tube has the same characteristics of those of the cabin evaporator, with eleven microchannels with 0.83 mm x 1.25 mm. We assume that the heat released by the battery is completely transferred to the heat exchanger and that the heat transfer within the battery in one-dimensional. In this sense, the top of the battery must have the highest temperature, T_b.

In the numerical model, we assume that the heat exchanger is divided into two-phase and superheated zones and the thermal resistance for each zone is

$$\frac{1}{UA} = \frac{l_b}{A_b k_b} + \frac{1}{\eta_r A_r h_r}. \tag{11}$$

Similarly to the condenser and cabin evaporator models, the convective heat transfer resistance is neglected in the two-phase zone, whereas in the single-phase zone it is calculated according to the constant heat flux condition for laminar flow and Gnielinski's correlation (Gnielinski, 1976) for turbulent flow. In the two-phase zone, since the temperature difference between the fluid and the battery remains constant, the heat transfer rate can be calculated simply as

$$Q = UA\left(T_b - T_e\right). \tag{12}$$

In the single-phase zone the fluid temperature varies along the heat exchanger. Therefore, the heat transfer rate is calculated as

$$Q = UA\Delta T_{lm}, \tag{13}$$

where ΔT_{lm} is the logarithmic mean temperature difference, calculated based on the temperature differences between the fluid and the top of the battery. At the beginning of the single-phase zone, $\Delta T_i = T_b - T_e$, where T_e stands for the evaporating temperature. At the evaporator outlet

$$\frac{\Delta T_o}{\Delta T_i} = \exp\left(-\frac{UA}{\dot{m}c_p}\right). \tag{14}$$

3. MATHEMATICAL MODEL OF THE BATTERY THERMAL LOAD

The thermal load of the battery evaporator is given by sum of the heat generated by each battery cell, which is calculated according to

$$\dot{Q} = Ri^2 - iT\frac{\Delta S}{nF}. \tag{15}$$

where R is the overpotential resistance, i is the cell electric current, T is the cell temperature, ΔS is the entropy change, n is the charge number, and F is the Faraday constant (Onda *et al.*, 2003). The first term on the right hand side represents the energy loss due to the charge transfer overpotential at the solid-electrolte interface, ohmic heat, and mass transfer limitations, whereas the second term represents the reversible entropy heat (Liu *et al.*, 2017).

The heat released by each battery cell is directly related to i, which depends on the battery output power, given by

$$\dot{W} = Vi = \frac{1}{\eta_t \eta_e}\left(mgfV + C_D\frac{\rho V^3 A}{2} + \delta m V\frac{dV}{dt}\right), \tag{16}$$

where η_t is the transmission efficiency, η_e is the energy efficiency of the power circuit, m is the mass of the vehicle, g is gravitational acceleration, f is the rolling resistance coefficient, V is the vehicle speed, C_D is the drag coefficient, ρ is the air density, A is the vehicle windward area, δ is the rotary mass conversion coefficient, and t is time. The cell current is obtained dividing the battery power output by its voltage.

In the present study, the following parameters were obtained from the BMW i3 datasheet (BMW, 2018): $m = 1710$ kg, $A = 2.38$ m^2, $C_D = 0.29$. All other input parameters required by Eq. (16), which were unavailable for the vehicle considered, were considered equal to those provided by Cen *et al.* (2018), that is, $\eta_t = 0.92$, $\eta_e = 0.99$, $f = 0.015$, and $\delta = 1.4$. The Samsung SDI 94Ah battery cells, with overpotential resistance of 0.93 mΩ and nominal voltage of 3.68 V (Samsung, 2015) were arranged in a 96S1P configuration, that is, with all 96 cells in series.

4. RESULTS

4.1 Prediction of battery heat generation

The BTMS performance analysis described in this study was conducted only for steady state condition. However, the heat generated by the battery module was initially predicted under typical unsteady operating conditions of the vehicle by means of Eqs. (15) and (16) considering the WLTC driving cycle for a class 3 vehicle. The results are shown in Figure 2, which indicate that the heat generation rate is under 1 kW in most part of the cycle, although it can reach up to around 2 kW for the medium and high speed parts of the cycle (suburban and rural scenarios) and 3 kW for the extra-high speed (highway scenario).

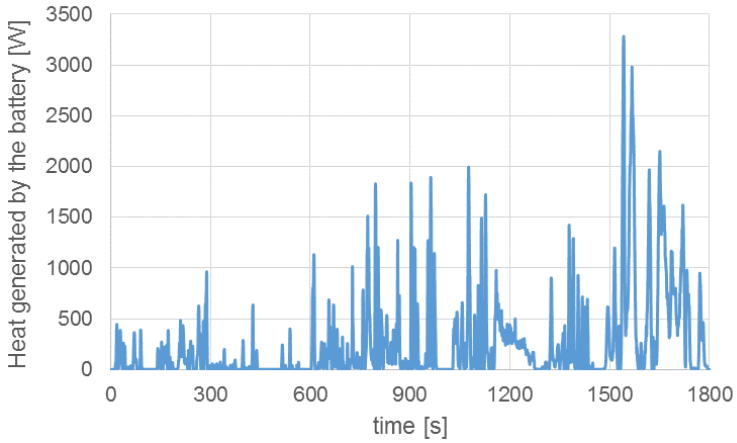

Figure 2. Instantaneous heat generation at the battery.

4.2 Performance analysis of the BTMS

The BTMS performance was evaluated under different operating conditions of compressor speed and battery heat generation, as shown in Figures 3 to 6. The cabin thermal load, the battery temperature, and the subcooling degree were assumed equal to 3 kW, 30 °C, and 30 °C, respectively. The latter has been defined as a high, but not limit, temperature in the 15 – 35 °C operational range suggested by Pesaran (2002) and Pesaran *et al.* (2013) for lithium-ion batteries. The thermodynamic state of air at the inlet of the heat exchangers are provided in Table 1. The expansion valves openings were adjusted to match the required cooling capacity in each evaporator.

Figure 3 shows how the BTMS power consumption is affected by the input parameters. Note that the curves are limited on the left by the minimum compressor speed that allows the system to achieve the required thermal load. It is seen that the power consumption increases continuously with the thermal load for a constant compressor speed, as expected. This parameter also increases considerably with the compressor speed for a constant thermal load. Therefore, it is clear that lower compressor speeds should be favored to increase the vehicle mileage. This is also verified in Figure 4, which shows

Table 1. Thermodynamic state of air at the inlet of the heat exchangers.

Condenser	**Value**
Air flow rate, kg/s	0.6
Air temperature, °C	30.0
Evaporator	**Value**
Air flow rate, kg/s	0.15
Air temperature, °C	30.0
Air relative humidity	0.5

how the COP (Coefficient of Performance) changes with the input parameters. In this figure, it is also noticed that the BTMS has a higher COP when the battery thermal load is around 1 to 2 kW.

Figures 5 and 6 show how the evaporation temperature and the superheating at the evaporator outlet change with compressor speed and battery thermal load. For a constant thermal load the evaporation temperature increases as the compressor speed decreases, which reduces the pressure ratio in the system and, consequently, increases the COP.

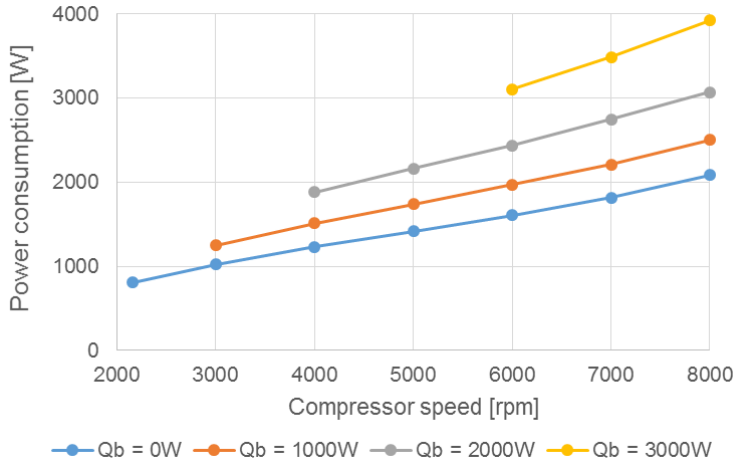

Figure 3. Power consumption as a function of compressor speed for different battery thermal loads (Q_b).

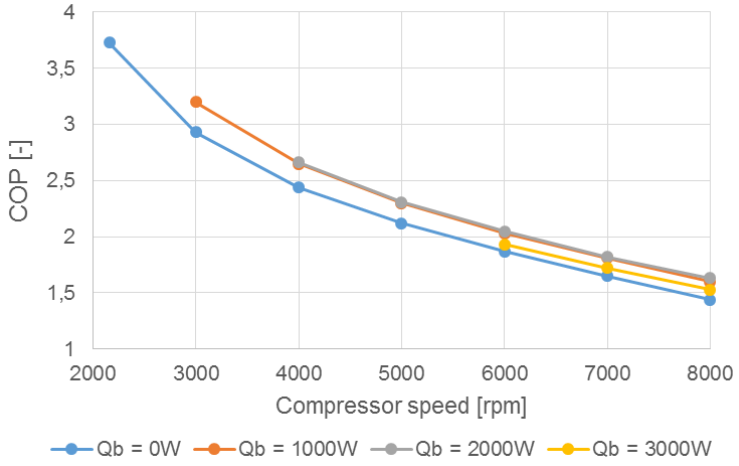

Figure 4. Coefficient of Performance as a function of compressor speed for different battery thermal loads (Q_b).

5. CONCLUSIONS

This study presents a comprehensive simulation model for direct refrigerant two-phase cooling systems applied for the thermal management of lithium-ion batteries used in electric vehicles. The compressor is represented by means of volumetric and overall isentropic efficiencies, the expansion device is described by an orifice equation and the heat exchangers are simulated using multi-zone models. These sub-models have been validated independently against experimental data

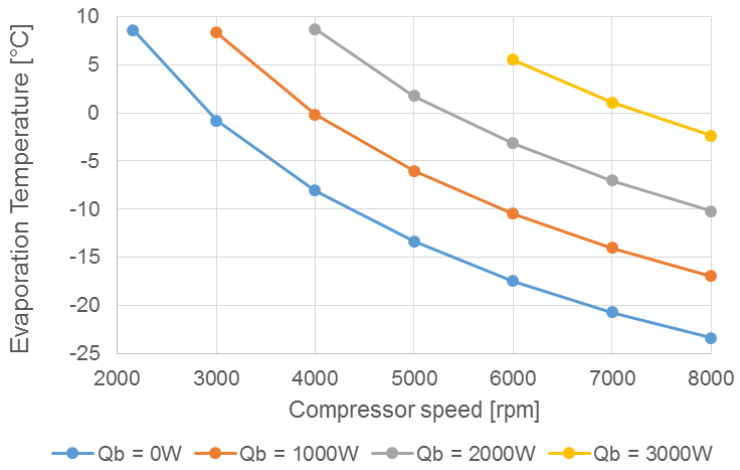

Figure 5. Evaporation temperature as a function of compressor speed for different battery thermal loads (Q_b).

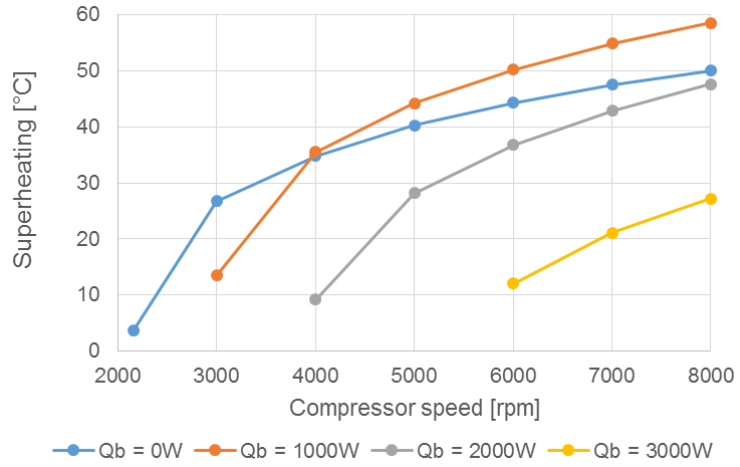

Figure 6. Superheating at the evaporator outlet as a function of compressor speed for different battery thermal loads (Q_b).

available in the literature, except for the battery evaporator. The compressor sub-model has maximum deviations of 1.9% and 3.4% for mass flow rate and power consumption, respectively, while the electronic expansion valve sub-model has a maximum deviation of 0.3% for mass flow rate. The heat exchangers sub-models have deviations of heat transfer rate lower than 2% for the condenser and average 6.5% for the evaporator. These components are integrated by means of the generic simulation model proposed by Zhu *et al.* (2013) for performance and control analysis of variable refrigerant flow (VRF) systems. A sensitivity analysis was conducted to verify how performance parameters change with the compressor speed and the heat generated in the battery. It is clear that the system COP increases when the compressor speed is reduced. Besides, the system reaches maximum COP values for a total thermal load in the range of 4 – 5 kW.

6. ACKNOWLEDGEMENTS

This work was funded by FAPESC under grant number 2022TR001385.

7. REFERENCES

BMW, 2018. "Technical specifications bmw i3 (120 ah)."

Cen, J., Li, Z. and Jiang, F., 2018. "Experimental investigation on using the electric vehicle air conditioning system for lithium-ion battery thermal management". *Energy for sustainable development*, Vol. 45, pp. 88–95.

Chang, Y.J. and Wang, C.C., 1997. "A generalized heat transfer correlation for iouver fin geometry". *International Journal of heat and mass transfer*, Vol. 40, No. 3, pp. 533–544.

Cuevas, C., Lebrun, J., Lemort, V. and Ngendakumana, P., 2009. "Development and validation of a condenser three zones model". *Applied Thermal Engineering*, Vol. 29, No. 17-18, pp. 3542–3551.

Datta, S., Das, P. and Mukhopadhyay, S., 2016. "Performance of a condenser of an automotive air conditioner with

maldistribution of inlet air—simulation studies and its experimental validation". *International Journal of Heat and Mass Transfer*, Vol. 98, pp. 367–379.

Ding, G.l., 2007. "Recent developments in simulation techniques for vapour-compression refrigeration systems". *International journal of refrigeration*, Vol. 30, No. 7, pp. 1119–1133.

Gnielinski, V., 1976. "New equations for heat and mass transfer in turbulent pipe and channel flow". *International chemical engineering*, Vol. 16, No. 2, pp. 359–367.

Jabardo, J.S., Mamani, W.G. and Ianella, M., 2002. "Modeling and experimental evaluation of an automotive air conditioning system with a variable capacity compressor". *International Journal of Refrigeration*, Vol. 25, No. 8, pp. 1157–1172.

Javani, N., Dincer, I., Naterer, G. and Rohrauer, G., 2014. "Modeling of passive thermal management for electric vehicle battery packs with pcm between cells". *Applied Thermal Engineering*, Vol. 73, No. 1, pp. 307–316.

Kim, J., Oh, J. and Lee, H., 2019. "Review on battery thermal management system for electric vehicles". *Applied thermal engineering*, Vol. 149, pp. 192–212.

Liu, H., Wei, Z., He, W. and Zhao, J., 2017. "Thermal issues about li-ion batteries and recent progress in battery thermal management systems: A review". *Energy conversion and management*, Vol. 150, pp. 304–330.

Nilpueng, K. and Wongwises, S., 2012. "A review of numerical modelling studies on short-tube orifice performance with applications to air-conditioning systems". *International journal of refrigeration*, Vol. 35, No. 4, pp. 740–749.

Onda, K., Kameyama, H., Hanamoto, T. and Ito, K., 2003. "Experimental study on heat generation behavior of small lithium-ion secondary batteries". *Journal of the Electrochemical Society*, Vol. 150, No. 3, p. A285.

Pesaran, A., Santhanagopalan, S. and Kim, G., 2013. "Addressing the impact of temperature extremes on large format li-ion batteries for vehicle applications (presentation)". Technical report, National Renewable Energy Lab.(NREL), Golden, CO (United States).

Pesaran, A.A., 2002. "Battery thermal models for hybrid vehicle simulations". *Journal of power sources*, Vol. 110, No. 2, pp. 377–382.

Samsung, 2015. "Intriduction of samsung sdi's 94ah cells."

Shi, J., Qu, X., Qi, Z. and Chen, J., 2011. "Investigating performance of microchannel evaporators with different manifold structures". *International Journal of Refrigeration*, Vol. 34, No. 1, pp. 292–302.

Shojaeefard, M., Molaeimanesh, G., Yarmohammadi, A. and Changizian, S., 2017. "Multi-objective optimization of an automotive louvered fin-flat tube condenser for enhancing hvac system cooling performance". *Applied Thermal Engineering*, Vol. 125, pp. 546–558.

Thomas, K.E. and Newman, J., 2003. "Thermal modeling of porous insertion electrodes". *Journal of the Electrochemical Society*, Vol. 150, No. 2, p. A176.

Zhao, Y., Liang, Y., Sun, Y. and Chen, J., 2012. "Development of a mini-channel evaporator model using r1234yf as working fluid". *International Journal of Refrigeration*, Vol. 35, No. 8, pp. 2166–2178.

Zhu, Y., Jin, X., Du, Z., Fan, B. and Fu, S., 2013. "Generic simulation model of multi-evaporator variable refrigerant flow air conditioning system for control analysis". *international journal of refrigeration*, Vol. 36, No. 6, pp. 1602–1615.

8. RESPONSIBILITY NOTICE

The authors are solely responsible for the printed material included in this paper.